Combinatorial search of thermoelastic shape-memory alloys with extremely small hysteresis width

JUN CUI[1,2]*, YONG S. CHU[3], OLUGBENGA O. FAMODU[2], YASUBUMI FURUYA[4], JAE. HATTRICK-SIMPERS[2], RICHARD D. JAMES[5], ALFRED LUDWIG[6,7], SIGURD THIENHAUS[6,7], MANFRED WUTTIG[2], ZHIYONG ZHANG[5] AND ICHIRO TAKEUCHI[2,8]

[1]Materials Analysis and Chemical Science, GE Global Research Center, Niskayuan, New York 12309, USA
[2]Department of Materials Science and Engineering, University of Maryland, College Park, Maryland 20742, USA
[3]Advanced Photon Source, Argonne National Laboratory, Argonne, Illinois 60439, USA
[4]Department of Intelligent Machines and Systems Engineering, Hirosaki University, Hirosaki 036-8561, Japan
[5]Department of Aerospace Engineering and Mechanics, University of Minnesota, Minneapolis, Minnesota 55455, USA
[6]Caesar Research Center, Ludwig-Erhard-Allee 2, 53175 Bonn, Germany
[7]Institut fur Werkstoffe, Ruhr-Universitat Bochum, 44780 Bochum, Germany
[8]Center for Superconductivity Research, University of Maryland, College Park, Maryland 20742, USA
*e-mail: cui@crd.ge.com

Published online: 5 March 2006; doi:10.1038/nmat1593

Reversibility of structural phase transformations has profound technological implications in a wide range of applications from fatigue life in shape-memory alloys (SMAs) to magnetism in multiferroic oxides. The geometric nonlinear theory of martensite universally applicable to all structural transitions has been developed. It predicts the reversibility of the transitions as manifested in the hysteresis behaviour based solely on crystal symmetry and geometric compatibilities between phases. In this article, we report on the verification of the theory using the high-throughput approach. The thin-film composition-spread technique was devised to rapidly map the lattice parameters and the thermal hysteresis of ternary alloy systems. A clear relationship between the hysteresis and the middle eigenvalue of the transformation stretch tensor as predicted by the theory was observed for the first time. We have also identified a new composition region of titanium-rich SMAs with potential for improved control of SMA properties.

Nitinol (nickel titanium naval ordnance laboratory) is a binary alloy with composition near 50 at.% Ni–50 at.% Ti. It is one of the most popular SMAs in medical applications owing to its biocompatibility and its remarkable properties that allow recoverable mechanical energy to be stored in a compact delivery system. It can retain the shape-memory effect following many cycles of deformation. Even though nitinol represents the best known SMA, its undesirable fatigue properties exemplified by the occurrence of medical-device fracture[1], along with large temperature/stress hysteresis and the narrow temperature range of operation translate to a tight margin of error for engineering design of the devices, and performance has been sacrificed for reliability. Accordingly, further incorporation of SMA into applications has been slow and limited despite its vast potential.

To this end, extensive research has been carried out to understand nitinol and to seek even better SMAs. Without a suitable theoretical guidance, the development of superior SMAs is largely based on trial and error. A new theory on the origin of reversibility of phase transformations has emerged[2–5]. The theory explains why martensites form microstructure and describes how this microstructure and the shape-memory effect are tied to the crystalline symmetry and geometric compatibilities. The theory further explains the fundamental cause of large transformation hysteresis commonly shown by SMAs, and predicts that the hysteresis can be drastically minimized by improving the geometric compatibility of the martensite and the austenite. In addition, hysteresis is a direct measure of the dissipated work,

which goes mainly into the creation of defects that subsequently become the sites of crack initiation[6]. Thus, by improving the geometric compatibility, SMA's resistance to fracture could also be greatly enhanced.

The theory specifies several conditions in order for a SMA to show extremely low hysteresis. Theoretical derivation of these conditions can be found in refs 4,5. The first condition is $\det\mathbf{U} = \lambda_1\lambda_2\lambda_3 = 1$ and the second condition is $\lambda_2 = 1$, where $\mathbf{U}$ is the transformation stretch tensor that maps the martensite lattice to the austenite lattice, $\det\mathbf{U}$ is its determinant and $\lambda_1 \leq \lambda_2 \leq \lambda_3$ are the ordered eigenvalues of $\mathbf{U}$. The form of the stretch tensor $\mathbf{U}$ can be derived if lattice parameters of both the austenite and the martensite phases and their symmetries are known. For example, there are six martensitic variants for a cubic-to-orthorhombic transformation. In the case of transformation through a face-diagonal stretch, the exact forms of the variants are

$$\mathbf{U}_1 = \begin{bmatrix} \beta & 0 & 0 \\ 0 & \frac{\alpha+\gamma}{2} & \frac{\alpha-\gamma}{2} \\ 0 & \frac{\alpha-\gamma}{2} & \frac{\alpha+\gamma}{2} \end{bmatrix}, \mathbf{U}_2 = \begin{bmatrix} \frac{\alpha+\gamma}{2} & 0 & \frac{\alpha-\gamma}{2} \\ 0 & \beta & 0 \\ \frac{\alpha-\gamma}{2} & 0 & \frac{\alpha+\gamma}{2} \end{bmatrix}, \mathbf{U}_3 = \begin{bmatrix} \frac{\alpha+\gamma}{2} & \frac{\alpha-\gamma}{2} & 0 \\ \frac{\alpha-\gamma}{2} & \frac{\alpha+\gamma}{2} & 0 \\ 0 & 0 & \beta \end{bmatrix},$$

$$\mathbf{U}_4 = \begin{bmatrix} \beta & 0 & 0 \\ 0 & \frac{\alpha+\gamma}{2} & \frac{\gamma-\alpha}{2} \\ 0 & \frac{\gamma-\alpha}{2} & \frac{\alpha+\gamma}{2} \end{bmatrix}, \mathbf{U}_5 = \begin{bmatrix} \frac{\alpha+\gamma}{2} & 0 & \frac{\gamma-\alpha}{2} \\ 0 & \beta & 0 \\ \frac{\gamma-\alpha}{2} & 0 & \frac{\alpha+\gamma}{2} \end{bmatrix}, \mathbf{U}_6 = \begin{bmatrix} \frac{\alpha+\gamma}{2} & \frac{\gamma-\alpha}{2} & 0 \\ \frac{\gamma-\alpha}{2} & \frac{\alpha+\gamma}{2} & 0 \\ 0 & 0 & \beta \end{bmatrix},$$

where $\alpha = a/a_0$, $\beta = b/a_0$, $\gamma = c/a_0$, and a_0 is the lattice parameter of the cubic austenite and a, b, c are the lattice parameters of orthorhombic martensite. $\mathbf{U}$ can be taken to be any one of these six matrices (they all have the same eigenvalues).

The first condition, $\det\mathbf{U} = 1$, means that there is no volume change due to the transformation. The significance of this condition on reversibility is an intuitive one, and it has been appreciated for a long time, although there have been no systematic quantitative studies.

The second condition, $\lambda_2 = 1$, means that the austenite is directly compatible with a single variant of martensite. During the phase transformation, martensitic variants and the austenite all have nearly the same free energy, and thus they can often coexist and form a complex arrangement of microstructures. A commonly observed microstructure for materials that do not satisfy $\lambda_2 = 1$ (the typical case) undergoing a martensitic phase transformation is alternating layers of two martensitic variants meeting a homogeneous region of austenite, as illustrated in Fig. 1. As is well understood from the crystallographic theory of martensite, the presence of this microstructure is due to the fact that in the typical case neither variant by itself is compatible with austenite, but a fine laminated mixture of variants is approximately compatible with austenite. The meeting place is a transition layer containing elastic energy, and the fineness of the microstructure is determined by a competition between the elastic energy stored in the transition layer and the interfacial energy on the twin boundaries between the variants. In fact, the branching of the twins at the interface, just visible in Fig. 1, is a further mechanism for reducing, but not eliminating, the elastic energy at the interface. In short, because of the incompatibility between austenite and martensite, there is both elastic and interfacial energy stored owing to the presence of the two phases. This occurs in both directions of the transformation, and the loading device used to apply biasing stress must overcome this additional free energy by supplying additional stress or, in the case of temperature change, the temperature must be raised sufficiently above the transformation temperature on heating, or below on cooling, to supply the additional free energy, leading to hysteresis. However,

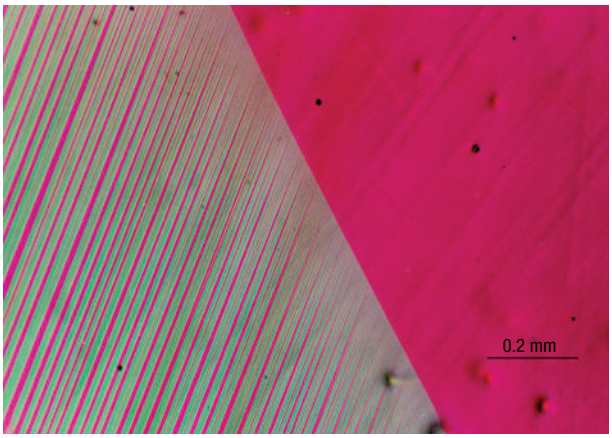

Figure 1 Microstructure of twinned martensite meeting a homogeneous region of austenite in a Cu–Al–Ni alloy. Image from ref. 5 with kind permission of Springer Science and Business Media.

if $\lambda_2 = 1$ there is no need for either the elastic transition layer or the fine array of twin bands. It is the elimination of this energy of incompatibility, which must be overcome both ways through the transformation, that gives rise to the reduction of the hysteresis.

The transition layers between austenite and martensite twins can be eliminated if the austenite and the martensite are crystallographically exactly compatible. In terms of microstructure, it means the whole martensite region consists of only one variant meeting the austenite. This is a rare case and requires an exact crystallographic match of the austenite and the martensite along certain crystallographic directions. Such a case may exist if and only if λ_2 of the transformation stretch tensor $\mathbf{U}$ equals one. The closer to one the λ_2 is, the more compatible the austenite and the martensite are, and thus the smaller the hysteresis is and the longer the fatigue life can potentially be. There are known compounds that come close to satisfying the above conditions. In particular, $Ni_{40.5}Ti_{49.5}Cu_{10}$ alloy has $\lambda_2 = 0.9986$ and $\det\mathbf{U} = 1.0002$. Its hysteresis is about 100 MPa and 20 °C, in terms of stress and temperature, respectively. These values are among the smallest reported so far[7].

Because the only inputs to the theory are lattice parameters, it can be used as a practical guide for the development of superior SMAs. The lattice parameters can be tuned by adjusting compositions, and the search of superior SMA is then simplified to mapping the lattice parameters versus compositions for a variety of alloy systems. The combinatorial approach provides an elegant solution to the task of mapping and tracking the lattice-parameter change across compositional phase diagrams, while monitoring to see if the hysteresis indeed changes in the predicted manner. We have thus implemented the combinatorial thin-film synthesis and characterization strategy (see Methods). Synchrotron X-ray microdiffraction and temperature-dependent resistance measurements were used to map the lattice parameters and the hysteresis behaviour, respectively. For the present investigation, we have focused on the Ni–Ti–Cu system because of one of its alloy is known to have a middle eigenvalue close to one[7]. Figure 2 shows the composition region of interest. In particular, the region inside the blue curve was mapped on our ternary composition-spread wafers.

It is known[7–12] that most alloys showing the shape-memory effect in the Ni–Ti–Cu system lie near 50 at.% Ti with Cu concentration varying from 0 to about 25 at.% as approximated by the strip outlined by a black line in Fig. 2. However,

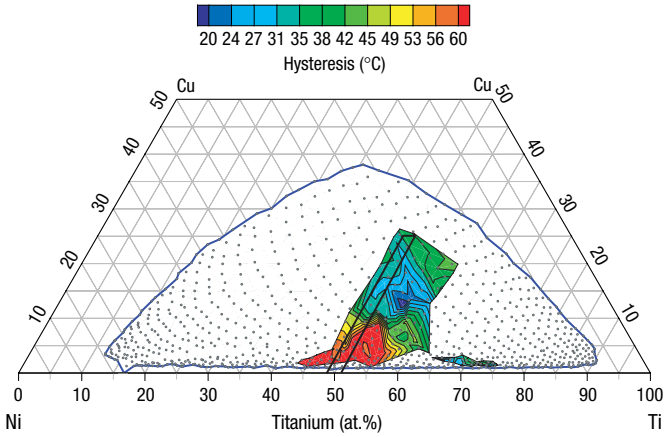

Figure 2 Transforming regions and thermal hysteresis in Ni–Ti–Cu. The small grey dots enclosed by a thick blue line represent the compositions being investigated.

the exact boundary of the shape-memory regions on the Ni–Ti–Cu phase diagram is not known. Although this study was not designed to address this question, it was able to provide an approximate answer. The figure shows the mapping result using colours ranging from red to blue to depict the shape-memory region and the associated hysteresis ranging approximately from 60 °C to 20 °C. Reversible martensitic transformations were characterized using temperature-dependent electrical resistance measurements ($R(T)$). The measurements yielded nearly, 2,000 $R(T)$ curves from one wafer. Although some curves clearly showed reversible transformations, others were less obvious. In Fig. 2, only the region with unambiguously discernible transformation behaviour as detected by $R(T)$ is shown. Yet the transforming region is already significantly extended from the previously known region near the 50 at.% Ti line.

The most notable feature of Fig. 2 is the green region (corresponding to the hysteresis value of ~35 °C) with titanium concentration varying from 65 to 77 at.% and Cu concentration varying from 0 to 4 at.%. Temperature-dependent synchrotron X-ray analysis of the film with 68 at.% Ti and 3 at.% Cu verified the reversible transformation. In addition, the X-ray patterns of compounds in this region also show the presence of a large volume fraction of Ti_2Ni precipitates. This is consistent with the high concentration of Ti in this alloy. Figure 3 depicts the X-ray-diffraction pattern of the alloy with composition $Ni_{35.4}Ti_{62.9}Cu_{1.7}$. The high-temperature pattern is indexed with two sets of lattice parameters, 11.278 Å cubic for the minor peaks and 3.010 Å cubic for the dominant peaks. The lattice parameters used to index the minor peaks match those of the compound Ti_2Ni, which is a known phase in the Ni–Ti alloy system and appears as a precipitate in the $Ni_{35.4}Ti_{62.9}Cu_{1.7}$ alloy. A further analysis is currently being carried out to determine the matrix composition, but, on the basis of the stoichiometry of the alloy, the titanium concentration of the matrix should not be too far away from 60 at.%. This is a potentially useful finding as the large fraction of precipitates promises for greater control of the overall shape memory properties, such as the transformation temperature and the stress magnitude of the superelasticity plateau.

To confirm this finding, two bulk samples with compositions $Ni_{35.4}Ti_{62.9}Cu_{1.7}$ and $Ni_{33.6}Ti_{65.2}Cu_{1.2}$ were prepared by arc melting. Differential scanning calorimetry has indicated that both alloys transform to austenite near 50 °C and to martensite near 75 °C,

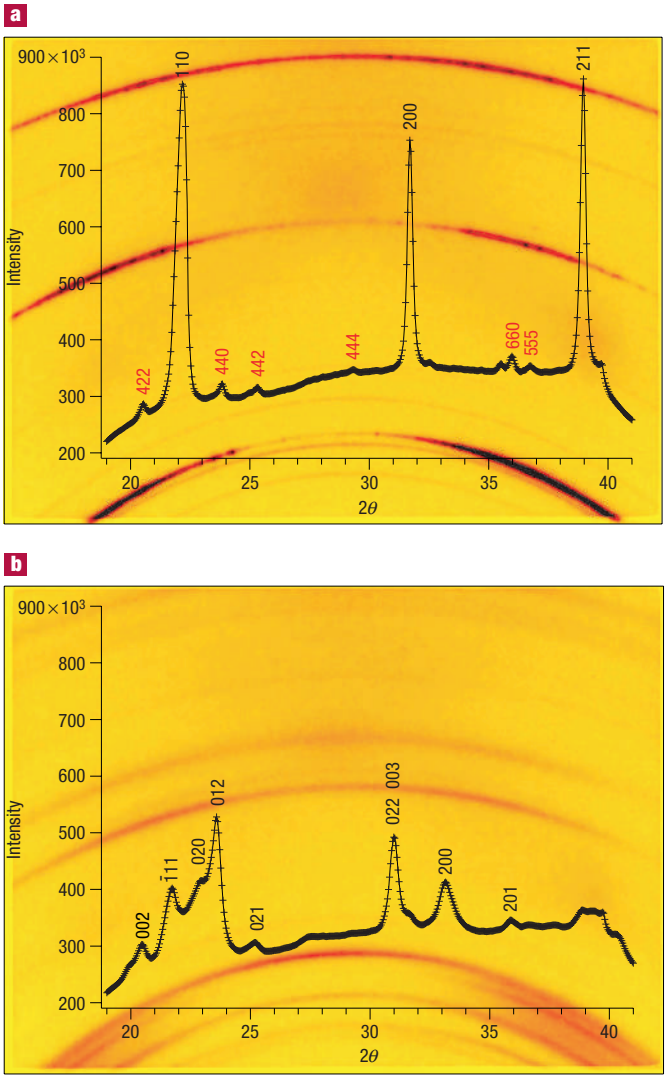

Figure 3 X-ray-diffraction images and integrated patterns of the spot with composition $Ni_{35.4}Ti_{62.9}Cu_{1.7}$. a,**b**, The images were taken at 135 °C (**a**) and 0 °C (**b**).

which are in good agreement with the transformation behaviour of the same compositions observed on the thin-film composition-spread wafer. Even though these alloys do not show the low hysteresis we are looking for, their lower Ni content and more adjustable SMA properties compared with the well-known Ni–Ti SMA composition is attractive for engineering applications. This finding is a good example of serendipitous discoveries made by the combinatorial approach.

Another important feature of Fig. 2 is the mapping of the thermal hysteresis. It shows that the composition with minimum hysteresis is located near 55 at.% Ti and 12 at.% Cu. Any departure from this composition results in an increase of the hysteresis, especially towards the lower copper concentration where zero copper concentration yields the largest hysteresis. It is interesting to compare this result with published data as in refs 7–9 and 13. Most of the Ni–Ti–Cu alloys previously studied have composition ranging from 47 to 52 at.% Ti and 0 to 25 at.% Cu, as indicated by the strip area in Fig. 2. In this area, the thermal hysteresis is reported to be decreasing with increasing Cu concentration before Cu reaches 10 at.%, and is more or less independent of

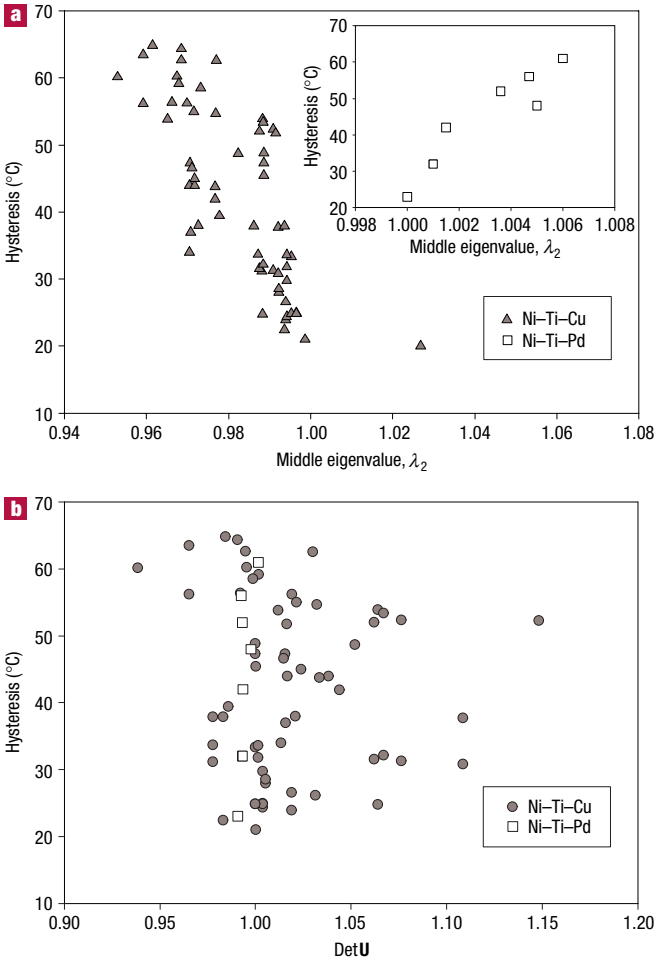

Figure 4 Transformation hysteresis in Ni–Ti–Cu. a,**b**, Hysteresis as a function of the middle eigenvalue (**a**) and as a function of the transformation stretch matrix (**b**). The inset in **a** shows, for comparison, the transformation hysteresis for Ni–Ti–Pd.

Cu concentration after 10 at.%. This result, as first reported by Hashinaga *et al.*[9], agrees with our result very well. As shown by Fig. 2, the strip area enclosed by the solid black line has hysteresis values varying from red to light blue (approximately 60 °C to 25 °C) with increasing Cu concentration before Cu reaches 10 at.%, indicating the hysteresis decreases with increasing Cu concentration. Once the Cu exceeds 10 at.%, the thermal hysteresis seems to become mostly independent of the Cu concentration.

To verify the criteria for minimum hysteresis, we plot in Fig. 4 the measured thermal hysteresis versus λ_2 (Fig. 4a) and det**U** (Fig. 4b) as defined above. The main plot of Fig. 4a shows the expected trend that the hysteresis decreases as the value of λ_2 approaches one. What was not expected is that most data points in the plot are located on the $\lambda_2 < 1$ side. Initially, we wondered if this observation of most of the Ni–Ti–Cu alloys having $\lambda_2 < 1$ is due to our thin-film synthesis method and not reflecting the intrinsic materials properties. To this end, 35 bulk-alloy samples were synthesized in the same composition range. The λ_2 values of these alloys were also found to lie in the $\lambda_2 < 1$ range. We therefore conclude that reversible martensites in the Ni–Ti–Cu system predominantly have lattice parameters with $\lambda_2 < 1$. In order to perform a quick check on the universality of this criterion for minimum hysteresis, we have also synthesized several alloys in the Ni–Ti–Pd system. The inset of Fig. 4a shows that this system also shows the trend of λ_2 versus hysteresis width predicted by the theory. Interestingly, however, λ_2 values of Ni–Ti–Pd alloys were found to all lie on the $\lambda_2 > 1$ side. On the basis of the present results, it seems to be the case that whether λ_2 values are mostly larger than 1 or smaller than 1 is a materials property particular to each alloy system. It was also found in the Ni–Ti–Pd alloys that the actual value λ_2 does not vary greatly as a function of composition, and a small variation of λ_2 seems to lead to a rather large change in the hysteresis width. This can be seen in the inset of Fig. 4a, where the sensitivity of the hysteresis to λ_2 is nearly one order larger than that for the Ni–Ti–Cu case.

Thus, we have validated the theoretical prediction of the hysteresis behaviour as a function of λ_2 using the two plots in Fig. 4a obtained from two alloy systems. However, there seems to be no obvious trend of hysteresis with det**U** (Fig. 4b), and investigation using bulk samples yielded similar results. It seems that the det**U** value is not as critical as λ_2 in determining the hysteretic behaviour.

As explained above on intuitive grounds, deviations from either of the conditions det$\mathbf{U} = 1$ and $\lambda_2 = 1$ are expected to increase the hysteresis. The common argument for the significance of det**U** is that, if, for instance, during transformation from austenite to martensite a nucleus of martensite were to grow in the matrix of austenite, then the volume mismatch and the elastic compatibility will necessarily cause the martensite to be surrounded by an elastically stressed layer, and *vice versa* for the reverse transformation. Accounting for the fact that transformation is a free-energy-decreasing process, the temperature on cooling will have to be lowered (and raised on heating) sufficiently to compensate for this excess free energy. Transformation initiating at a stress-free surface can decrease the energy stored in this transition layer, but it is unlikely to eliminate it. The finding here seems to therefore contradict the conventional wisdom. Explaining this striking result represents a future theoretical challenge.

The present experiment underscores the effectiveness of the combinatorial approach in systematically validating phenomenological theories that relate diverse properties of materials. The present study would have taken a very long time by bulk synthesis and characterization techniques. Having revealed the significance of $\lambda_2 = 1$ in this study, we can now use this criterion together with combinatorial methods to discover new highly reversible alloys. Mapping of other ternary alloy systems are currently under way.

Because the theory addresses the reversibility of structural transitions in general, it has far-reaching applicability to a variety of functional materials showing structural transitions. Other physical properties whose changes can be closely associated with phase transitions include hydrogen solubility, thermal and electrical resistivity, optical transparencies, luminescence and thermoelectricity. We can apply the same experimental technique described here to control and optimize the hysteresis behaviour in various physical properties in respective functional materials by fine-tuning the lattice parameters through composition variation guided by the theory.

METHODS

Thin-film composition spreads of the Ni–Ti–Cu ternary alloy system were prepared using an ultra-high-vacuum magnetron co-sputtering system on 3-inch Si wafers (400 μm thick) with 400 nm SiO_2 layers. Three 1.5-inch-diameter sputtering guns were placed parallel and adjacent to each other in a triangular configuration. By adjusting the power applied to each gun and the distance between the guns and the wafer, different regions of the ternary phase diagram could be mapped. The spread films with thicknesses 0.5–0.75 μm were deposited at room temperature followed by a 2 h anneal in vacuum at

550 °C. The spreads were deposited through a metal mask grid, which separates the film into 800 1.5×1.5 mm^2 squares. Wavelength dispersive spectroscopy was used to map the compositions of every square for each wafer. Further details of the composition-spread synthesis scheme can be found in ref. 14.

To evaluate the substrate effect imposed on the properties of SMA films, several composition spreads were released and lifted from the original Si/SiO_2 wafers and then embedded into a soft polymer matrix. The films on the polymer matrix, however, did not show any significant departure in structural properties (as determined by X-ray diffraction) from the films on Si/SiO_2 wafers. It was concluded that the post-deposition heat treatment relaxes stresses to the extent that lattice-parameter values measured with and without substrates agree within our experimental error. In light of this finding, all measurements were performed on the original Si/SiO_2 wafers.

The thermal hysteresis was measured on the wafer using the principle that SMA films show changes in electrical resistance due to phase transformation[15]. The electrical resistance was mapped by scanning the entire library with a four-point probe at a constant temperature. The mapping was then repeated at various temperatures from −20 to 100 °C, then back to −20 °C with a 2 °C increment. Following the measurement, electrical resistance versus temperature curves $R(T)$ for each composition were constructed, and the transformation temperatures and their hysteresis were determined from these curves. To define the hysteresis, four phase-transformation temperatures were determined for each composition in the library: they were martensite starting and finishing temperatures during the cooling, M_s and M_f, and austenite starting and finishing temperatures during the heating, A_s, A_f. Among these four temperatures, M_s and A_f were much easier to identify than M_f and A_s: electrical resistivity changed abruptly when the material transformed from pure austenite to an austenite/martensite mixture or from the mixture back to pure austenite. Because of the good reliability in determination of M_s and A_f, we chose to define the hysteresis as $A_f - M_s$, which reflects the temperature difference of transformations to and from the pure austenite state. This definition of hysteresis ignores the possible presence of the intermediate R phase: it is possible that for some part of the library the hysteresis determined using this definition is for transformation from the B2 to B19 or to B19′ phases, whereas some part can be from B2 to R. However, the latter is known to be a small contribution to the hysteresis.

Characterization of the crystal structure of thin-film samples was carried out using the synchrotron X-ray microdiffraction at the beamline 2-BM of the Advanced Photon Source, Argonne National Laboratory. Nine minutes per spot was enough to obtain sufficient diffraction data for complete lattice parameter analysis on our textured thin-film samples. In this study, the beam size was focused to 0.01×0.01 mm^2 using Kirkpatric–Baez mirrors, and the photon energy was set to 15 keV. A charge-coupled-device camera was positioned at $2\theta = 34°$ and 65 mm from the sample. The camera recorded images at three different angles, 10°, 12° and 14°, and at two different temperatures, 135 °C and 0 °C. The exposure time of each image was 3 min. An algorithm was developed to convert the images to diffraction patterns. It was calibrated using the National Institute of Standards and Technology CeO_2 standard, and the result was verified using silicon powder. Example images and integrated diffraction patterns are shown in Fig. 3. Lattice parameters were extracted from these diffraction patterns, and then used to calculate the transformation stretch tensors and their determinant det**U** and the middle eigenvalue λ_2.

Bulk samples of the Ni–Ti–Cu and Ni–Ti–Pd ternary-alloy systems were prepared using a conventional arc-melting method. Each sample was melted, flipped and melted again five times. The samples obtained were then sealed in quartz tubes that were vacuumed and back-filled with argon gas. The argon-protected samples were then homogenized at 1,000 °C for 7 days followed by quenching in water. Lattice parameters and thermal hysteresis of the obtained samples were characterized using a Scintag XDS 2000 diffractometer and a TA Instruments Q1000 differential scanning calorimeter, respectively.

Received 1 September 2005; accepted 11 January 2006; published 5 March 2006.

References

1. Allie, D. E., Hebert, C. J. & Walker, C. M. Nitinol stent fractures in the SFA. *Endovasc. Today* **7,** 22–34 (2004).
2. Bhattacharya, K., Conti, S., Zanzotto, G. & Zimmer, J. Crystal symmetry and the reversibility of martensitic transformations. *Nature* **428,** 55–59 (2004).
3. Bhattacharya, K. & James, R. D. The material is the machine. *Science* **307,** 53–54 (2005).
4. Ball, J. M. & James, R. D. Proposed experimental tests of a theory of fine microstructure and the two well problem. *Phil. Trans. R. Soc. Lond. A* **338,** 389–450 (1992).
5. James, R. D. & Zhang, Z. in *Magnetism and Structure in Functional Materials* (eds Mañosa, L., Planes, A. & Saxena, A.) (Springer Series in Materials Science, Vol. 79, Springer, New York, 2005).
6. Kato, H., Ozu, T., Hashimoto, S. & Miura, S. Cyclic stress–strain response of superelastic Cu-Al-Mn alloy single crystals. *Mater. Sci. Eng. A* **264,** 245–253 (1999).
7. Miyazaki, S. & Ishida, A. Martensitic transformation and shape memory behavior in sputterdeposited TiNi-base thin films. *Mater. Sci. Eng. A* **273–275,** 106–133 (1999).
8. Nam, T. H., Saburi, T. & Shimizu, K. Cu-content dependence of shape memory characteristics in Ti-Ni-Cu alloys. *Mater. Trans. JIM* **31,** 959–967 (1990).
9. Hashinaga, T., Miyazaki, S., Ueki, T. & Horikawa, H. Transformation and deformation behavior in sputter-deposited Ti-Ni-Cu thin films. *J. Phys. IV* **5,** C8 689–C8 694 (1995).
10. Miyazaki, S., Hashinaga, T. & Ishida, A. Martensitic transformations in sputter-deposited Ti-Ni-Cu shape memory alloy thin films. *Thin Solid Films* **281–282,** 364–367 (1996).
11. Fukuda, T., Saburi, T., Chihara, T. & Tsuzuki, Y. Mechanism of B2-B19-B19′ transformation in shape memory Ti–Ni–Cu alloys. *Mater. Trans. JIM* **36,** 1244–1255 (1995).
12. Bricknell, R. H., Melton, K. N. & Mercier, O. The structure of NiTiCu shape memory alloys. *Metall. Trans. A.* **10,** 693–699 (1979).
13. Tang, W., Sandstrom, R., Wei, Z. G. & Miyazaki, S. Experimental investigation and thermodynamic calculation of the Ti-Ni-Cu shape memory alloys. *Metall. Mater. Trans. A* **31,** 2423–2430 (2000).
14. Takeuchi, I. *et al.* Identification of novel compositions of ferromagnetic shape memory alloys using composition spreads. *Nature Mater.* **2,** 180–184 (2003).
15. Faulkner, M. G., Amalra, J. J. & Bhattacharyya, A. Experimental determination of thermal and electrical properties of NiTi shape memory wires. *Smart Mater. Struct.* **9,** 632–639 (2000).

Acknowledgements

This work was supported by ONR-N000140110761, ONR-N000140410085, NSF DMR-0231291, NSF DMS-0074043 and MRSEC DMR-0520471. Use of the Advanced Photon Source was supported by the US Department of Energy, Office of Science, Office of Basic Energy Sciences, under Contract No W-31-109-Eng-38.
Correspondence and requests for materials should be addressed to J.C.

Competing financial interests

The authors declare that they have no competing financial interests.